

Construction of Neuroanatomical Shape Complex Atlas from 3D Brain MRI

Ting Chen¹, Anand Rangarajan¹, Stephan J. Eisenschenk², and Baba C. Vemuri¹ *

¹ Department of CISE, University of Florida, Gainesville, FL 32601, USA

² Department of Neurology, University of Florida, Gainesville, FL 32601, USA
{tichen, anand, vemuri}@cise.ufl.edu, stephan.eisenschenk@neurology.ufl.edu

Abstract. This paper proposes a novel technique for constructing a neuroanatomical *shape complex* atlas using an information geometry framework. A shape complex is a collection of shapes in a local neighborhood. We represent the boundary of the entire shape complex using the zero level set of a distance function $S(\mathbf{x})$. The spatial relations between the different anatomical structures constituting the shape complex are captured via the distance transform. We then leverage the well known relationship between the stationary state wave function $\psi(\mathbf{x})$ of the Schrödinger equation $-\hbar^2 \nabla^2 \psi + \psi = 0$ and the eikonal equation $\|\nabla S\| = 1$ satisfied by any distance function $S(\mathbf{x})$. This leads to a one-to-one map between $\psi(\mathbf{x})$ and $S(\mathbf{x})$ and allows for recovery of $S(\mathbf{x})$ from $\psi(\mathbf{x})$ through an explicit mathematical relationship. Since the wave function can be regarded as a square-root density function, we are able to exploit this connection and convert shape complex distance transforms into probability density functions. Furthermore, square-root density functions can be seen as points on a unit hypersphere whose Riemannian structure is fully known. A shape complex atlas is constructed by first computing the Karcher mean $\bar{\psi}(\mathbf{x})$ of the wave functions, followed by an inverse mapping of the estimated mean back to the space of distance transforms in order to realize the atlas. We demonstrate the shape complex atlas computation via a set of experiments on a population of brain MRI scans. We also present modes of variation from the computed atlas for the control population to demonstrate the shape complex variability.

1 Introduction

In the past two decades, human brain MRI analysis has attracted immense attention for the purposes of diagnosis and treatment of neurological diseases. In this context, the construction of neuroanatomical shape atlases of the human brain has been of particular interest and its importance has been emphasized in a number of recent studies [1]. In brief, an atlas provides a reference shape or image for a population of shapes/images which can be useful in numerous applications including but not limited to, statistical analysis of the populations,

* This research is in part supported by the NIH grant RO1 NS046812 to BCV & AR and the NSF grant RI-IIS 0954032 to BCV .

the segmentation of the structures of interest and the detection of the disease regions based on the shape variations between the atlas and the subject etc. Most existing atlases are based on isolated, single anatomical shapes [11, 10, 12] which do not contain any inter-structural information for example, the spatial relationships among different neighboring structures and the effect of volume shrinkage or expansion of structures in its neighborhood. However, many neurological disorders are diagnosed by the structural abnormalities (e.g. volume change) ascribed to several brain structures rather than a single structure. Mania, which is most often associated with bipolar disorder serves as an example, as in [2] all the brain structures associated with the neural pathways were examined and the authors claimed that the patients with mania have a significant *overall* volume difference in the regions including the thalamus, hippocampi and the amygdala. In [3], Seidman *et al.* concluded that one remarkable vulnerability of schizophrenia, is the structural abnormalities in the thalamus and the amygdala-hippocampus region. Therefore, a neuroanatomical shape complex atlas which captures the structural relationships will be of primary clinical importance.

2 Previous Work

In the context of atlas construction for multiple brain structures, most of the efforts in the past were focussed on building full brain *image* atlases. For instance, in [5, 4], several image atlas construction methods for the entire brain were proposed based on 3-D brain MRI. However, it is a nontrivial task to extend these techniques to shape atlas construction. Therefore, we will not be discussing these image based methods any further in this paper and only focus on shape atlas construction instead. One of the most common shape representations in the literature is to represent shapes using feature point sets or landmarks. As in [6], several research articles on point set atlas construction for anatomical structures (e.g. hippocampi) have been published where they model the shapes using mixture of densities and estimate the unbiased shape atlas via information theoretic methods. In [8], Cootes *et al.* developed a diffeomorphic statistical shape model which analyzes the parameters of the deformation field instead of the traditional landmark positions. Other methods that represent shapes in 2D using parametric curves or in 3D using parametric surfaces have also received considerable attention in the literature [7]. Since statistical shape analysis in curve/surface space is very difficult, methods using this representation have usually resorted to computing means etc. of spline parameters. In [9], a characteristic 3D shape model dubbed the m-rep, is proposed and based on this representation, an atlas is constructed via computation of the Karcher mean of the population [10]. Recent work in [11] describes an interesting model for continuous spherical shapes used to analyze the anatomical shape differences in the hippocampus of control group and blind subjects.

To summarize, in all the techniques discussed thus far, the shape atlas is developed only for a single structure. *In this paper, we propose a novel technique for constructing an atlas of a neuroanatomical shape complex of multiple*

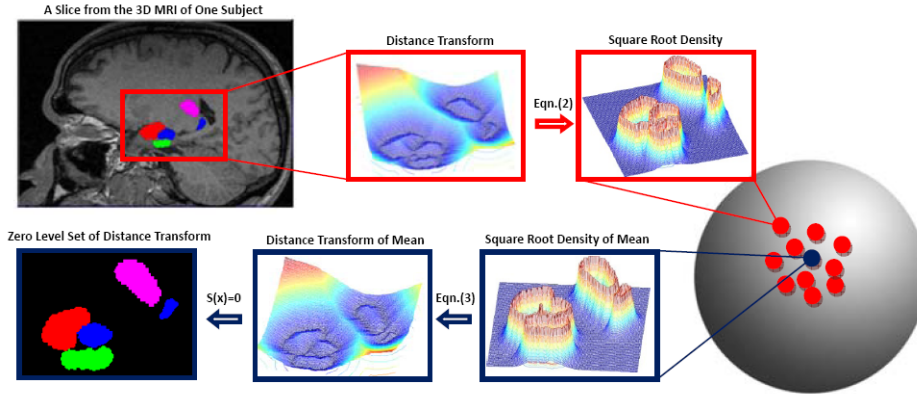


Fig. 1. Illustration of our framework. We visualize the distance transform and square-root density in the 2-D case. Each sample data turns out to be a red point on the high dimensional sphere and the blue point is the Karcher mean.

structures. The novelty lies in the relationship we exploit between the stationary state wave function $\psi(\mathbf{x})$ of the Schrödinger equation $-\hbar^2 \nabla^2 \psi + \psi = 0$ and the eikonal equation $\|\nabla S\| = 1$ for the Euclidean distance transform problem which serves as a “bridge” that connects the distance transform representation of the shape to its square-root-density. The choice of a square-root density representation is motivated by the fact that the manifold of square root densities is a unit Hilbertian sphere and its geometry is well understood. This allows us to use the intrinsic geometry of the sphere to compare shapes represented by square-root densities. Additionally, the inter-structural relationship is well captured in our distance transform representation of the shape complex. In section 4, we demonstrate our technique by presenting examples of atlas construction for the shape complex of 8 structures from a population of 15 3-D brain MRI with all the structures labeled by an expert neurologist.

3 Shape Complex Atlas

3.1 From Distance Transforms to Square-Root Density Functions

In our model, each shape complex data sample is represented by the distance transform function, the zero level set of which gives the individual boundaries of the various shapes constituting the shape complex. At least two decades of effort have gone into level set and distance function representations of shapes [13] - the principal advantage being the ability to combine different shapes into a single scalar field representation. However, since variational and partial differential equation methods are at the foundation of level sets, it is a non-trivial task to employ statistical methods on scalar field distance function representations. Alternatively, there exists a class of methods that perform shape analysis by representing single shapes using probability density functions [6], and obtaining

very good results. For instance, despite sacrificing the ability to represent a set of shapes or a shape complex, in this framework, the mean, variance and principal modes of the shape population are all easily computed. One of the main contributions of this paper is to successfully *bridge* the two disparate domains - variational and level set methods on the one hand and probabilistic methods on the other - and directly obtain the density function of a shape complex from a distance function representation.

In [15], Gurumoorthy and Rangarajan apply the Schrödinger equation to the Euclidean distance transform problem. They solve the Schrödinger wave equation instead of the corresponding static Hamilton-Jacobi equation for the distance transform. While they emphasize the main advantage of their approach to be the linearity of the Schrödinger equation (as opposed to the non-linearity of the Hamilton-Jacobi equation), we wish to draw upon the obvious, historical precedent in quantum mechanics of motivating the Schrödinger wave function as a square-root density [16]. Inspired by this voluminous previous work, we adopt the interpretation of the stationary state Schrödinger wave function for the Euclidean distance function as a square-root density.

Let $\psi(\mathbf{x})$ be the stationary state wave function and let \hbar - Planck's constant - be a free parameter in this model. The static wave equation for the Euclidean distance function problem is³

$$\hbar^2 \nabla^2 \psi(\mathbf{x}) = \psi(\mathbf{x}). \quad (1)$$

CLAIM: When $\psi(\mathbf{x}) = \alpha \exp(\frac{-S(\mathbf{x})}{\hbar})$ and satisfies Eqn. (1), $S(\mathbf{x})$ asymptotically satisfies the eikonal equation $\|\nabla S\| = 1$ as $\hbar \rightarrow 0$. Here α is a normalization constant such that $\psi(\mathbf{x})$ is a square-root density, i.e. $\int \psi^2(s) ds = 1$.

PROOF: From the definition of a square-root density, $\alpha^2 = \frac{1}{\int \exp(\frac{-2S(\mathbf{x})}{\hbar}) d\mathbf{x}}$, which is a constant for each $S(\mathbf{x})$. Taking the 2-D case as an example, when $\psi(x_1, x_2) = \alpha \exp(\frac{-S(x_1, x_2)}{\hbar})$, we have the second partials for the Laplacian as

$$\begin{aligned} \frac{\partial^2 \psi}{\partial x_1^2} &= \frac{\alpha}{\hbar^2} \exp(\frac{-S}{\hbar}) \left(\frac{\partial S}{\partial x_1}\right)^2 - \frac{\alpha}{\hbar} \exp(\frac{-S}{\hbar}) \frac{\partial^2 S}{\partial x_1^2} \\ \frac{\partial^2 \psi}{\partial x_2^2} &= \frac{\alpha}{\hbar^2} \exp(\frac{-S}{\hbar}) \left(\frac{\partial S}{\partial x_2}\right)^2 - \frac{\alpha}{\hbar} \exp(\frac{-S}{\hbar}) \frac{\partial^2 S}{\partial x_2^2}. \end{aligned}$$

From Eqn.(1), we have $(\frac{\partial S}{\partial x_1})^2 + (\frac{\partial S}{\partial x_2})^2 - \hbar(\frac{\partial^2 S}{\partial x_1^2} + \frac{\partial^2 S}{\partial x_2^2}) = 1$ which implies

$$\|\nabla S\|^2 - \hbar \nabla^2 S = 1.$$

Since $\nabla^2 S$ is bounded, we obtain $\|\nabla S\| = 1$ as \hbar goes to 0.

END

The derivation above allows us to recover the distance transform function from the square-root density representation by computing the inverse map of

$$\psi(\mathbf{x}) = \alpha \exp(\frac{-S(\mathbf{x})}{\hbar}), \quad (2)$$

³ Please see [15] for a more detailed derivation.

that is

$$S(\mathbf{x}) = \hbar \log(\alpha) - \hbar \log(\psi(\mathbf{x})). \quad (3)$$

This important relationship builds a direct connection between the two realms, i.e. the level set framework and probability density functions. Hence, a shape complex of complicated topology can be represented using a single distance transform function and further statistical analysis of the shape population can be accomplished in the space of the unit hypersphere as a result of a transition from the distance function to the square-root density representation.

3.2 Space of Square-Root Densities

Note that Eqn. (1) does not entail that the solution is a square-root density. Rather, it merely builds a relationship between exponentiated distance functions and the Schrödinger equation. We further restrict the solution to be in the square-root density space via Eqn. (2) and Eqn. (3). The principal reasons for focusing on the square-root density space rather than the exponentiated function space is as follows.

- Probability density functions are very useful shape representations as shown by several researchers in the literature. For instance, one can compute moments of the density and get global/local shape descriptors [18] while this cannot be done with an un-normalized exponentiated distance function. One can also match either the densities or their moments for the purpose of registration.
- Probability density functions allow us to relate our unknown parameter (Planck’s constant) \hbar to uncertainty.
- Furthermore, the space of exponentiated functions is positive semidefinite while the square-root density space is the hypersphere which leads to a closed form metric (and geodesic) that is efficient to compute.

Due to the fact that the manifold for square-root density functions is a unit sphere in Hilbert space, a variety of Riemannian operations, such as geodesic distance, exponential map and log map [17] are in closed form. Equipped with this basic infrastructure, we are now able to construct an atlas for the shape complex by computing the Karcher mean of the given shape complex population in the space of unit hypersphere. We illustrate the idea of our framework on a simple example in Fig.1. Note that here the notion of atlas corresponds to the mean computed from the the L^2 norm. However, any norm is applicable in our framework, for example, estimating the median of the population via the L^1 norm. As a matter of fact, with the square-root density representation, we are capable of performing many different kinds of statistical analysis.

4 Experimental Results

In this section, we demonstrate the strength of our technique via a set of experiments on a population of real shape complex data. The images are affine

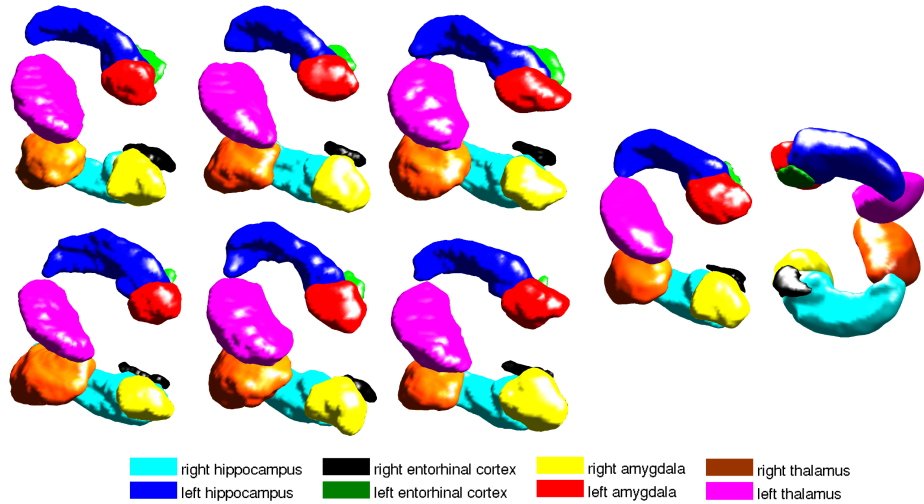


Fig. 2. 6 samples from the group of 15 subjects and the two different views of the atlas with $\hbar = 0.4$

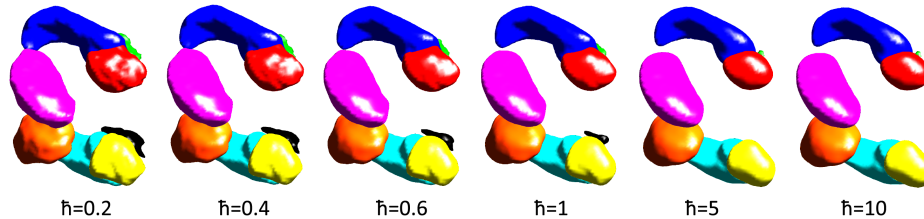


Fig. 3. Atlas corresponding to different \hbar values. As \hbar increases, the atlas becomes more smooth.

registered using an ITK-based mutual information registration algorithm [14]. Before going into the details of the experimental results, we first clarify two empirical issues related to the experiments.

De-normalization of $\bar{\psi}$: Since $\bar{\psi}(\mathbf{x})$ is the geodesic mean on the sphere of the sample square root densities, it is valid to assume that $\psi(\mathbf{x})$ has the same formulation as each shape complex data sample (represented by $\psi_i(\mathbf{x}) = \alpha_i \exp(\frac{-S_i(\mathbf{x})}{\hbar})$, $i = 1, \dots, n$), that is, $\bar{\psi}(\mathbf{x}) = \bar{\alpha} \exp(\frac{-\bar{S}(\mathbf{x})}{\hbar})$. Therefore, $\bar{S}(\mathbf{x}) = -\hbar \log(\bar{\psi}(\mathbf{x})) + \hbar \log(\bar{\alpha})$.

To recover $\bar{S}(\mathbf{x})$, we first need to estimate $\bar{\alpha}$. One approach is to heuristically approximate $\log(\bar{\alpha})$ using the average of $\log(\alpha_1), \dots, \log(\alpha_n)$. Here we describe a more principled solution. Assume $\phi(\mathbf{x}) = \exp(\frac{-S(\mathbf{x})}{\hbar})$, is the un-normalized version of ψ (the exponentiated function). Note that we lose one degree of freedom by normalization, hence an extra constraint needs to be imposed. We approximate $\bar{\psi}(\mathbf{x})$ by the linear combination of the un-normalized density ϕ due to the linearity imposed by Eqn. (1). The problem is finally reduced to solve $b^* = \arg \min_{\mathbf{b}} \|\sum_{i=1}^n b_i \phi_i(\mathbf{x}) - \bar{\psi}(\mathbf{x})\|^2$. This assumption is in accordance with

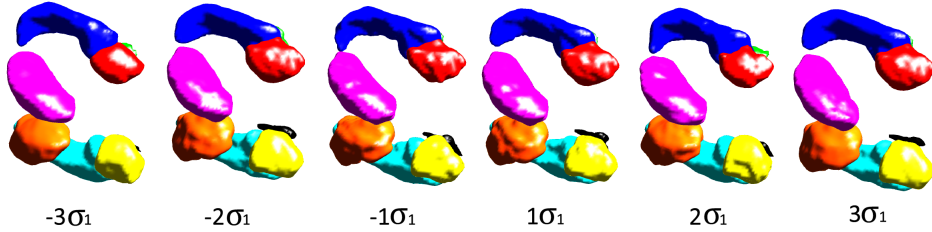


Fig. 4. The shape variation along the first principal direction.

the observation that the density has peaks on the locations corresponding to the zero level set of the distance function. The normalization parameter $\bar{\alpha}$ is approximated using $\sum_i b_i^*$ and it scales the un-normalized exponentiated distance function so that we can obtain a zero-level set shape complex atlas. Since this is just one way of obtaining a zero-level set atlas, a numerically more stable flux-based method might be a better future work direction.

Visualization: We transfer the labels of each structure in the shape complex by mapping the label image to our atlas. (This is done only for visualization purposes.) The transformation parameters of the mapping is computed by a non-rigid warping from a binary image of the shape complex template to the binary image estimated from the shape atlas. We leave the automatic labeling of the shape complex atlas for future work.

In Fig. 1, we illustrate the idea of our framework on a simple 2-D example. The 2-D image is taken from one slice of the 3-D MRI of the shape complex. The flowchart shows that we first estimate the distance transform from the shape and then compute the square-root density via Eqn. (2). The shape of the atlas is recovered from the Karcher mean of the densities via Eqn. (3).

We finally apply our proposed framework to the real shape complex data set. The data set contains 15 controls of 3-D brain MRI with the following 8 structures labeled: left/right hippocampus, entorhinal cortex, amygdala and thalamus. We show 6 samples from the group of 15 subjects and the atlas constructed as the mean shape in two different angles of view in Fig. 2. While we have not emphasized this in our presentation, the parameter \hbar acts as a smoothing/regularization term for atlas construction and is expected to act as an uncertainty control - similar to the role played by Planck's constant in physics. We demonstrate the variation of the atlas when different \hbar is used in Fig.3. As \hbar increases, the atlas becomes more smooth. In this paper, we fix $\hbar = 0.4$ in the experiments. When Principal Geodesic Analysis [10] is applied to our data set, we can recover the modes of deformation and the shape variation along the first principal direction is shown in Fig. 4.

We implemented this method using Matlab® on a 2.33GHZ PC. It takes 4 minutes to construct an atlas from 15 labeled brain MRI with dimension of the ROI being $90 \times 91 \times 87$. This serves to anecdotally illustrate the computational time involved.

5 Conclusions

In this paper, we presented a novel and efficient algorithm that constructs a neuroanatomical atlas for shape complex data with complicated topology. We derived the relationships between the Euclidean distance transform and the square-root density wave function representation and this successfully builds on a connection between the realms of the level set framework and probability density functions. Our model is not only capable of preserving the spatial relationships among the different structures in the shape complex but also of carrying out a variety of statistical analyses of the shape complex population.

References

1. B. T. T. Yeo *et al.*, “Effects of registration regularization and atlas sharpness on segmentation accuracy”. *Medical Image Analysis*, 12(5):603-615, 2008.
2. S. M. Strakowski *et al.*, “Brain magnetic resonance imaging of structural abnormalities in bipolar disorder”. *Arch Gen Psychiatry*, 56(3):254-60, Mar, 1999.
3. L. J. Seidman *et al.*, “Thalamic and amygdala/hippocampal volume reductions in first-degree relatives of patients with schizophrenia: an MRI-based morphometric analysis”. *Biological Psychiatry*, 46(7):941-954, Oct 1, 1999.
4. S. Gerber, T. Tasdizen, S. Joshi, R. Whitaker, “On the Manifold Structure of the Space of Brain Images”. *MICCAI*, 12(Pt 1):305-312, 2009.
5. M. R. Sabuncu, M. E. Shenton, P. Golland, “Joint Registration and Clustering of Images”. *MICCAI Stat. Reg. Workshop*, 47-54, 2007.
6. T. Chen *et al.*, “Group-wise Point-set registration using a novel CDF-based Hausdorff-Charvat Divergence”. *IJCV*, 86(1):111-124, 2010.
7. T. B. Sebastian, J. J. Crisco, P. N. Klein, B. B. Kimia, “Constructing 2D Curve Atlases”. *IEEE Workshop on MMBIA*, 70-77, 2000.
8. T. F. Cootes, C. J. Twining, K. O. Babalola, C. J. Taylor, “Diffeomorphic Statistical Shape Models”. *Image and Vision Computing*, 26:326-332, 2008.
9. M. Styner *et al.*, “Statistical Shape Analysis of Neuroanatomical Structures Based on Medial Models”. *Medical Image Analysis*, 7:207-220, 2003.
10. P. Fletcher, C. Lu, S. Pizer, S. Joshi, “Principal geodesic analysis for the study of nonlinear statistics of shape”. *IEEE Trans Med Imaging*, 23(8):995-1005, 2004.
11. X. Liu *et al.*, “Models of normal variation and local contrasts in hippocampal anatomy”. *MICCAI*, 2008.
12. L. Wang *et al.*, “Abnormalities of hippocampal surface structure on very mild dementia of the alzheimer type”. *NeuroImage*, 30(1):52-60, 2006.
13. R. Malladi, J. A. Sethian, B. C. Vemuri, “Shape modeling with front propagation: a level set approach”. *PAMI*, 17(2):158-175, February, 1995.
14. P. Thevenaz, M. Unser, “Optimization of Mutual Information for Multiresolution Image Registration”. *IEEE Trans Image Processing*, 9:2083-2099, 2000.
15. K. Gurumoorthy, A. Rangarajan, “A Schrödinger equation for the fast computation of approximate euclidean distance functions”. *SSVM*, 5567:100-111, 2009.
16. M. Born, “Zur Quantenmechanik der Stoßvorgänge”. *Zeitschrift für Physik A Hadrons and Nuclei*, 37(12):863-867, December, 1926.
17. A. Peter, A. Rangarajan, J. Ho, “Shape L’Ane Rouge: Sliding wavelets for indexing and retrieval”. *CVPR*, 2008.
18. J. Ho, A. Peter, A. Ranganranjan, M. Yang, “An Algebraic Approach to Affine Registration of Point Sets”. *ICCV*, 2009.